Li *et al. Biological Procedures Online* (2025) 27:13
https://doi.org/10.1186/s12575-025-00275-4

Biological Procedures Online

RESEARCH Open Access

Construction of a circRNA-miRNA-mRNA Regulatory Network for the Immune Regulation of Lung Adenocarcinoma

Hanyi Li[1,2†], Xin Jin[1,2†], Wei Li[1,2†], Fan Ren[1,2], Tong Li[1,2], Xuanguang Li[1,2], Haochuan Yu[1,2], Dianxun Fu[3], Zuoqing Song[1,2*] and Song Xu[1,2*]

Abstract

Background Recent research has highlighted the significance of circular RNAs (circRNAs) as pivotal regulators in the progression of tumors and the therapeutic response in non-small cell lung cancer (NSCLC). These circRNAs function through a sponge mechanism, interacting with microRNAs (miRNAs) to modulate mRNA expression levels. Nevertheless, the precise role of the circRNA-miRNA-mRNA regulatory network in immune regulation within lung adenocarcinoma (LUAD) remains inadequately understood.

Methods and Materials We utilized microarray datasets from the GEO NCBI database (GSE101586) to identify differentially expressed circRNAs (DEcircRNAs) in LUAD. CircBank was employed to predict the target miRNAs of DEcircRNAs, which were subsequently intersected with miRNAs from the GSE36681 database. The identified miRNAs were then predicted to target mRNAs using miRDB and miWalk, and intersections with immune-related genes from the IMMPORT database were analyzed. Protein-protein interaction (PPI) networks were constructed using Cytoscape software. The DAVID functional annotation tool was utilized to explore potential biological processes, molecular functions, and KEGG pathways associated with LUAD. Gene expression and Kaplan-Meier survival analyses were conducted to establish a key regulatory network and to assess immune cell infiltration and Pearson correlation for significant target genes. Finally, we selected the most significantly upregulated circRNA with differential expression for validation through in vitro experiments.

Results Our analysis identified a total of 7 upregulated and 42 downregulated circRNAs, along with 10 significant miRNAs and 20 target mRNAs. KEGG enrichment analysis indicated that these components are primarily enriched in the ErbB signaling pathway. Furthermore, Gene Ontology (GO) analysis revealed significant enrichment in responses to organic substances, cytokine-mediated signaling pathways, cellular responses to cytokines, responses to chemical stimuli, steroid hormone receptor activity, ErbB-3 class receptor binding, oxysterol binding, signal receptor activity, and molecular transducer activity. Notable core mRNAs identified included OAS1, VIPR1, and PIK3R1. Subsequently,

[†]Hanyi Li, Xin Jin and Wei Li contributed equally to this work.

*Correspondence:
Zuoqing Song
thoracic_expert@aliyun.com
Song Xu
xusong198@hotmail.com

Full list of author information is available at the end of the article

we constructed a regulatory network comprising 6 DEcircRNAs, 3 DEmiRNAs, and 3 DEmRNAs. Through ssGSEA and CIBERSORT analyses, we observed significant differences in immune cell infiltration levels between the NSCLC cohort and the control group. Knocking down the expression of hsa_circ_0079557 significantly inhibited the viability, proliferation, migration, and invasion of LUAD cells.

Conclusion We have established a circRNA-miRNA-mRNA regulatory network that offers novel insights into the molecular mechanisms governing immune regulation in LUAD. Future research should aim to translate these findings into clinical applications to enhance patient outcomes.

Keywords Lung adenocarcinoma, Circular RNA, Prognosis, Immune infiltration

Introduction

Non-small cell lung cancer (NSCLC) represents the most prevalent form of tumor disease, with approximately 40% of diagnosed cases classified as lung adenocarcinoma (LUAD) [1]. The current limitations in lung cancer screening methodologies, coupled with the delayed onset of clinical symptom, often result in diagnoses occurring at advanced stages. Presently, the five-year survival rate for lung cancer remains below 15% [2]. Consequently, there is an urgent imperative for comprehensive research into lung adenocarcinoma to uncover novel therapeutic targets and diagnostic biomarkers.

Circular RNAs (circRNAs) were first identified in 1976 and are known to be associated with certain viral pathogens [3]. As a form of non-coding RNA, circRNAs are characterized by their covalently closed loop structure, which lacks a poly(A) tail at the 3' end and a cap structure at the 5' end. This distinctive configuration endows circRNAs with a prolonged half-life and enhanced resistance to RNase R degradation compared to linear RNAs [4], thereby presenting significant potential for application in cancer diagnosis and treatment. Previous studies have demonstrated that circ-CPA4 influences the growth, activity, stemness, and drug resistance of NSCLC cells, as well as the activation of CD8 + T cells within the tumor immune microenvironment, through the let-7 miRNA/PD-L1 axis [5]. Additionally, circ_POLA2 has been shown to regulate the stemness and progression of lung cancer cells by modulating the miR-326/GNB1 axis, indicating its potential as a novel therapeutic target for lung cancer patients [6]. Furthermore, N6-adenosine-modified circIGF2BP3 has been found to inhibit the CD8 + T cell response by promoting the deubiquitination of PD-L1 in non-small cell lung cancer, thereby facilitating tumor immune evasion [7]. Thus, investigating the underlying molecular mechanisms of LUAD is crucial for enhancing diagnostic and therapeutic strategies for patients.

Lung cancer growth and development are complex and dynamic processes, involving the inherent genetic abnormalities of tumor tissues and the interaction between the tumor tissue and local microenvironmental immune cells [8]. UPP1 is demonstrated to enhance the infiltration of antitumor T cells and is potentially linked with the tumor microenvironment (TME) [9]. Additionally, the loss of PTEN leads to the development of an immunosuppressive microenvironment in lung cancer, contributing to immunotherapy resistance in LUSC [10].Therefore, it is vital to identify immune-related differentially expressed RNAs (DEmRNAs) in LUAD to further elucidate potential molecular mechanisms. This study aims to identify immune-related DEmRNAs, DEmiRNAs, and DEcircRNAs in LUAD utilizing the GEO database. We constructed a circRNA-miRNA-mRNA regulatory network based on the identified DEmRNAs, DEmiRNAs, and DEcircRNAs to explore potential molecular immune regulatory mechanisms mediated by circRNA-miRNA-mRNA interactions.

Methods and Materials

Microarray Datasets

The microarray dataset containing circular RNA (circRNA) and microRNA (miRNA) expression profiles from human lung cancer samples was sourced from the Gene Expression Omnibus (GEO) database (http://www.ncbi.nlm.nih.gov/geo/). Specifically, we selected the GSE101586 dataset, which encompasses five female patients diagnosed with lung adenocarcinoma who have no history of smoking. This dataset was analyzed for circRNA expression through microarray technology. Paired tumor and adjacent non-tumor tissues were collected and subsequently validated by a pathologist. Additionally, the GSE36681 dataset was utilized for miRNA expression analysis, which included 47 pairs of formalin-fixed, paraffin-embedded (FFPE) tissues from non-smokers, matched between lung adenocarcinoma and unaffected lung tissues.

Differential Expression Analysis and Venn Analysis

Differentially expressed circRNAs (DEcircRNAs) and miRNAs (DEmiRNAs) were identified using the limma package in R. The criteria for differential expression included combined effect sizes (ES) greater than 1 and a false discovery rate (FDR) of less than 0.05. For significant differential expression, the thresholds were set at|log2(FC)| greater than 1 and an adjusted p-value of less than 0.05. Immune-related mRNAs were retrieved

from the IMMPORT database (https://www.immport.org/shared/home). DEcircRNAs underwent miRNA prediction via the CircBank online tool, and the resulting target miRNAs were subsequently intersected with DEmiRNAs from the GSE36681 dataset. The identified miRNAs were then utilized to predict target mRNAs through the miRDB and miWalk online platforms. These predicted mRNAs were further intersected with DEmRNAs and immune-related mRNAs for Venn analysis, resulting in a final list of mRNAs. DEmiRNAs were obtained from the GEPIA2 database (http://gepia2.cancer-pku.cn), while immune-related mRNAs were sourced from the IMMPORT database (https://www.immport.org/shared/home).

Definition of miRNA-Related Prognostic Model

To validate the DEmiRNAs within the subnetworks, we employed the kmplot online database (https://kmplot.com/analysis/) to assess the intersected miRNAs, ultimately identifying significant miRNAs, with a p-value threshold of greater than 0.05 deemed significant.

Construction of PPI Network, GO and KEGG Pathway Analysis

A protein-protein interaction (PPI) network for the target differentially expressed genes (DEGs) was constructed using the STRING online tool (https://cn.string-db.org/). For gene set functional enrichment analysis, we utilized the KEGG REST API (https://www.kegg.jp/kegg/rest/keggapi.html) to obtain the most recent gene annotations for KEGG pathways, which served as the background reference. Genes were mapped to this background set, and enrichment analysis was conducted using the R package clusterProfiler (version 3.14.3) to derive the results of the gene set enrichment analysis. The minimum gene set size was established at 5 and the maximum at 5000, with a p-value of less than 0.05 and an FDR of less than 0.25 considered statistically significant. For gene set functional enrichment analysis, gene GO annotations from the R package org.Hs.eg.db (version 3.1.0) were utilized as the background. The mapping and enrichment analysis were performed similarly, adhering to the same criteria for statistical significance.

Differential Expression and Survival Analysis of Human Genes

Differential expression data for these hub genes in lung adenocarcinoma (LUAD) tissues compared to normal tissues were obtained from The Cancer Genome Atlas (TCGA). The influence of these hub genes on overall survival (OS) rates in lung cancer was assessed using the Gene Expression Profiling Interactive Analysis (GEPIA, http://gepia2.cancer-pku.cn/), a web-based tool derived from TCGA data.

Immune Cell Infiltration

The CIBERSORT and ssGSEA methodologies were utilized to evaluate the distribution and relative proportions of different immune cell types present within the samples. Concurrently, the Tumor Immune Estimation Resource (TIMER, http://timer.cistrome.org/) was employed to investigate the relationship between gene expression and the infiltration of various immune cell types.

Patients and Samples

The samples utilized in this study were sourced from patients who had undergone surgical treatment at Tianjin Medical University General Hospital and had been pathologically diagnosed with LUAD or benign lesions. The clinical characteristics of the patients are provided in Table S1 of Supplementary Material 1. A total of 42 blood samples were collected from LUAD patients and 7 from patients with benign lesions. (Benign lesions patients refer to individuals whose resected pulmonary lesions were pathologically confirmed as non-malignant tumors. In this study, we collected peripheral blood samples from patients including 3 cases of pulmonary hamartoma, 2 cases of tuberculosis, and 2 cases of intrapulmonary lymph node involvement.) It is noteworthy that all patients included in the study had not undergone radiotherapy or chemotherapy prior to surgery, ensuring the purity of the samples and the accuracy of the research findings. The study was approved by the Ethics Committee of Tianjin Medical University General Hospital, and informed consent was obtained from all patients.

Cell Culture

We purchased human lung epithelial cells (BEAS-2B) and LUAD cells (H1299, A549) from the American Tissue Culture Collection (ATCC). The BEAS-2B, H1299, and A549 cells were cultured in RPMI-1640 medium (Gibco, Grand Island, NY, USA) supplemented with 10% fetal bovine serum (FBS) at 37 °C in an environment containing 5% CO2.

Reverse Transcription Quantitative PCR

TRIzol® reagent (Invitrogen; Thermo Fisher Scientific) was utilized for RNA extraction. Subsequently, the PrimeScript™ RT-PCR Kit (Accurage Biology) was employed following the manufacturer's protocol. The thermal cycler block system (Takara Bio), in conjunction with SYBR Green PCR Master Mix (Thermo Fisher Scientific), facilitated the PCR reactions. Customized primer sequences for circRNA were synthesized by Shanghai Luhe Huada Genomics Co., Ltd., with GAPDH serving as an internal control for circRNA normalization. (The primer sequences can be found in Table S2 of the Supplementary Material 1.) The thermal cycling conditions comprised an initial step at 95 °C for 15 min, followed by

cycles of 15 s at 94 °C, 30 s at 55 °C, and 30 s at 70 °C. Following the PCR procedure, the relative expression levels were calculated using the $2-\Delta\Delta Cq$ method. The experiment was independently replicated three times to ensure reproducibility.

CCK-8 Assay

Twenty-four hours post-transfection, cells were seeded into 96-well plates at a density of 4×10^3 cells per well. Five replicate wells were established for each experimental group, along with a blank control group. On days 0, 1, 2, and 3 of culture, 10 μL of CCK-8 reagent was added to the designated wells. The plate was subsequently incubated in a light-protected environment for 1 h, followed by measurement of absorbance at 450 nm using a microplate reader. Data were processed by excluding the highest and lowest values within each group. The mean of the remaining values was calculated and normalized against the blank control group to generate cell growth curves, which were subjected to subsequent statistical analysis.

Clone Formation Assay

Cells in the logarithmic growth phase from each group were collected, digested routinely, and centrifuged to obtain a cell pellet. Subsequently, a complete culture medium containing 10% serum was used to prepare a cell suspension. Cells from each group were then seeded into 6-well plates at a density of 1.5 × 10^3 cells per well. The 6-well plates were placed in a cell incubator at 37 °C with 5% CO2 for continued culture.After the desired incubation period, the original culture medium in each well was discarded, and the cells were carefully washed twice with pre-cooled 1×PBS. Next, 1 mL of 4% paraformaldehyde was added to each well to fix the cells for 15 min. Following fixation, the cells were stained with 1% crystal violet staining solution for 30 min and then rinsed gently with running water to remove excess stain. Finally, the 6-well plates were allowed to air-dry.

Western Blotting

The experiment employed RIPA lysis buffer (sourced from Thermo Fisher Scientific) for sample preparation. Protein quantification was conducted using the BCA Protein Assay Kit (also from Thermo Fisher Scientific), with each lane loaded with 8 micrograms of protein. Subsequently, PVDF membranes (supplied by Thermo Fisher Scientific) were blocked with 5% non-fat milk at room temperature for one hour, followed by overnight incubation with the primary antibody at 4 °C. Afterward, the membranes were incubated with HRP-conjugated goat anti-rabbit IgG (H + L) at 37 °C. The protein bands were analyzed using ImageJ software. The entire experiment was replicated three times to ensure reproducibility.

Statistical Methods

To ensure the reliability of the experimental results, each experiment was conducted at least three times, with comprehensive data collection from all trials. We utilized GraphPad 9 software as our statistical analysis tool and for the creation of charts and graphs. When comparing data between two groups, Student's t-test was applied: a P-value less than 0.05 was considered indicative of a statistically significant difference between the two groups, whereas a P-value less than 0.01 was deemed to suggest a highly statistically significant difference.

Results

Identification of immune-related DEcircRNAs、DEmiRNA, and DEmRNA

We retrieved a total of 4,425 circular RNAs (circRNAs) from the GSE101586 database and 1,145 microRNAs (miRNAs) from the GSE36681 database, with their corresponding heatmaps presented in Fig. 1A-B. From this data, we identified seven significantly upregulated circRNAs and 42 downregulated circRNAs, selected based on substantial expression differences ($|logFC| \geq 1.5$). The detailed information regarding these circRNAs is provided in Supplementary Material 2.

CircRNAs are known to perform various biological functions. Numerous studies have established that circRNAs function as competing endogenous RNAs (ceRNAs) or miRNA sponges [11, 12]. Accordingly, utilizing the circBank database, we identified target miRNAs that can bind to the significantly upregulated and downregulated DEcircRNAs. We then intersected the target miRNAs of the upregulated DEcircRNAs with both the upregulated and downregulated DEmiRNAs from the GSE36681 database, and similarly for the downregulated DEcircRNAs. To further refine our selection of significant miRNAs, we conducted Kaplan-Meier survival analysis on the intersecting miRNAs, identifying those of clinical relevance as illustrated in Fig. 2. Utilizing the miWalk and miRDB databases, we predicted downstream mRNAs for these significant miRNAs and intersected them with immune-related genes and DEmRNAs obtained from the GEPIA online database for non-small cell lung cancer, resulting in the identification of 20 mRNAs: OAS1, RORC, PIK3R1, ILK, VIPR1, SEMA6A, RORA, DUOX2, TNFAIP3, NRG1, S1PR1, IL1RL1, NR2C2, CCRL2, TGFBR3, PIK3R1, TFRC, CCL22, PAK6, and HNF4G, as depicted in Fig. 3.

Construction of PPI Network and GO/KEGG Enrichment Analysis

To elucidate the interactions among the identified mRNAs, we constructed a PPI network (Fig. 4A). We performed GO and KEGG enrichment analyses on these genes, revealing that within the molecular function

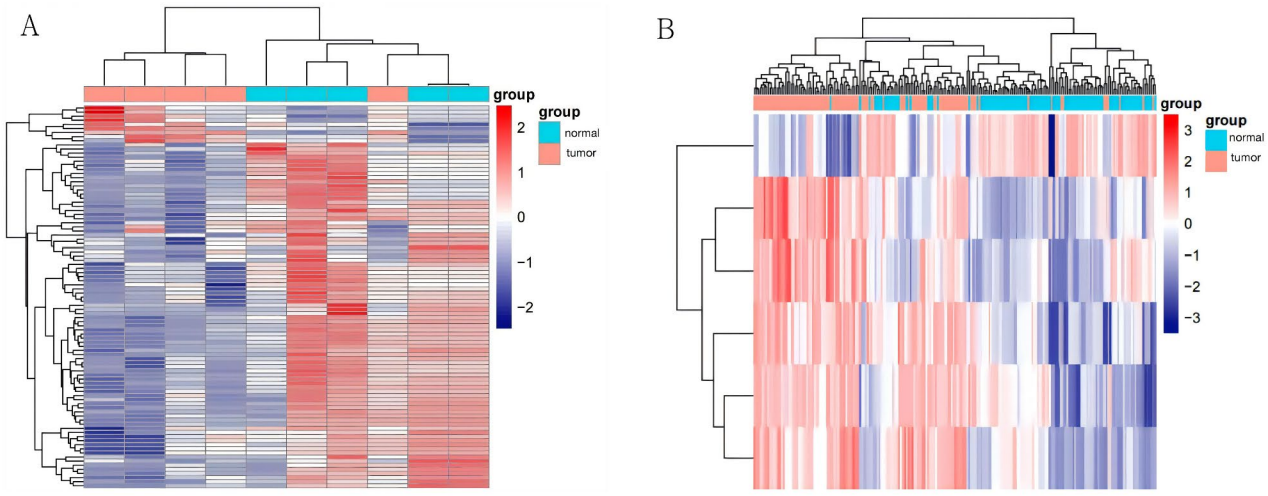

Fig. 1 Heatmaps of the top DEcircRNA (**A**) and all DEmiRNAs (**B**) in LUAD

category, these genes were predominantly enriched in the following activities: cellular response to organic substances, cytokine-mediated signaling pathways, cellular response to cytokines, cellular response to chemicals, steroid hormone receptor activity, binding to ErbB-3 type receptors, oxysterol binding, signaling receptor activity, and molecular transducer activity, among others (Fig. 4B-D). The KEGG enrichment analysis indicated a primary enrichment in the ErbB signaling pathway.

Construction of Regulatory Network

We conducted tissue expression and survival analyses of the identified mRNAs using the TCGA database, ultimately identifying significant core mRNAs, specifically OAS1, VIPR1, and PIK3R1, as illustrated in Fig. 5. Subsequently, we constructed a regulatory network comprising six DEcircRNAs, three DEmiRNAs, and three DEmRNAs, which includes the following interactions: hsa_circ_0079557-hsa-miR-502-5p-OAS1, hsa_circ_0000370-hsa-miR-502-5p-OAS1, hsa_circ_0000369-hsa-miR-502-5p-OAS1, hsa_circ_0020390-hsa-miR-502-5p-OAS1, hsa_circ_0023685-hsa-miR-542-3p-VIPR1/PIK3R1, and hsa_circ_0001666-hsa-miR-193a-3p-PIK3R1, as depicted in Fig. 6.

Correlation between Immune Cell Infiltration and Central Immune-Related DEmRNAs

Utilizing ssGSEA and CIBERSORT analyses, we observed significant differences in immune cell infiltration levels between the LUAD group and the control group (Fig. 7A-B). These differentially infiltrated immune cells were found to be associated with the central immune-related DEmRNAs (Fig. 7C). A comprehensive analysis revealed a significant correlation between the expression levels of three genes—OAS1, VIPR1, and PIK3R1—and the infiltration of various immune cell types in LUAD, including B cells, CD4 + T cells, CD8 + T cells, neutrophils, macrophages, and dendritic cells. The results indicate that the expression levels of VIPR1 and PIK3R1 (as illustrated in Fig. 7D) are positively correlated with B cells, CD4 + T cells, CD8 + T cells, macrophages, and dendritic cells. Consequently, we hypothesize that elevated expression of VIPR1 and PIK3R1 may enhance antitumor immunity within the LUAD microenvironment. This hypothesis is further substantiated by the observation of improved survival rates in patients exhibiting increased expression of the VIPR1 and PIK3R1 genes. Conversely, our findings did not demonstrate a significant association between OAS1 gene expression and immune cell infiltration, suggesting that OAS1 may function as an oncogene that potentially inhibits antitumor immune responses, thereby adversely affecting patient survival.

The Expression of hsa_circ_0079557 is Increased in LUAD Cells, and Knockdown of hsa_circ_0079557 Inhibits Cell Proliferation and Migration

To validate our conclusions, we randomly selected a circRNA, hsa_circ_0079557, for in-depth investigation. Experimental results demonstrated that the expression level of hsa_circ_0079557 in LUAD cells was markedly elevated compared to normal BEAS-2B cells, with particularly notable differences observed in A549 cells (Fig. 8A). Furthermore, through real-time fluorescent quantitative polymerase chain reaction (qPCR) analysis of blood samples from patients, we found that the expression level of hsa_circ_0079557 was significantly higher in these patients compared to those with benign nodules (Fig. 8B).

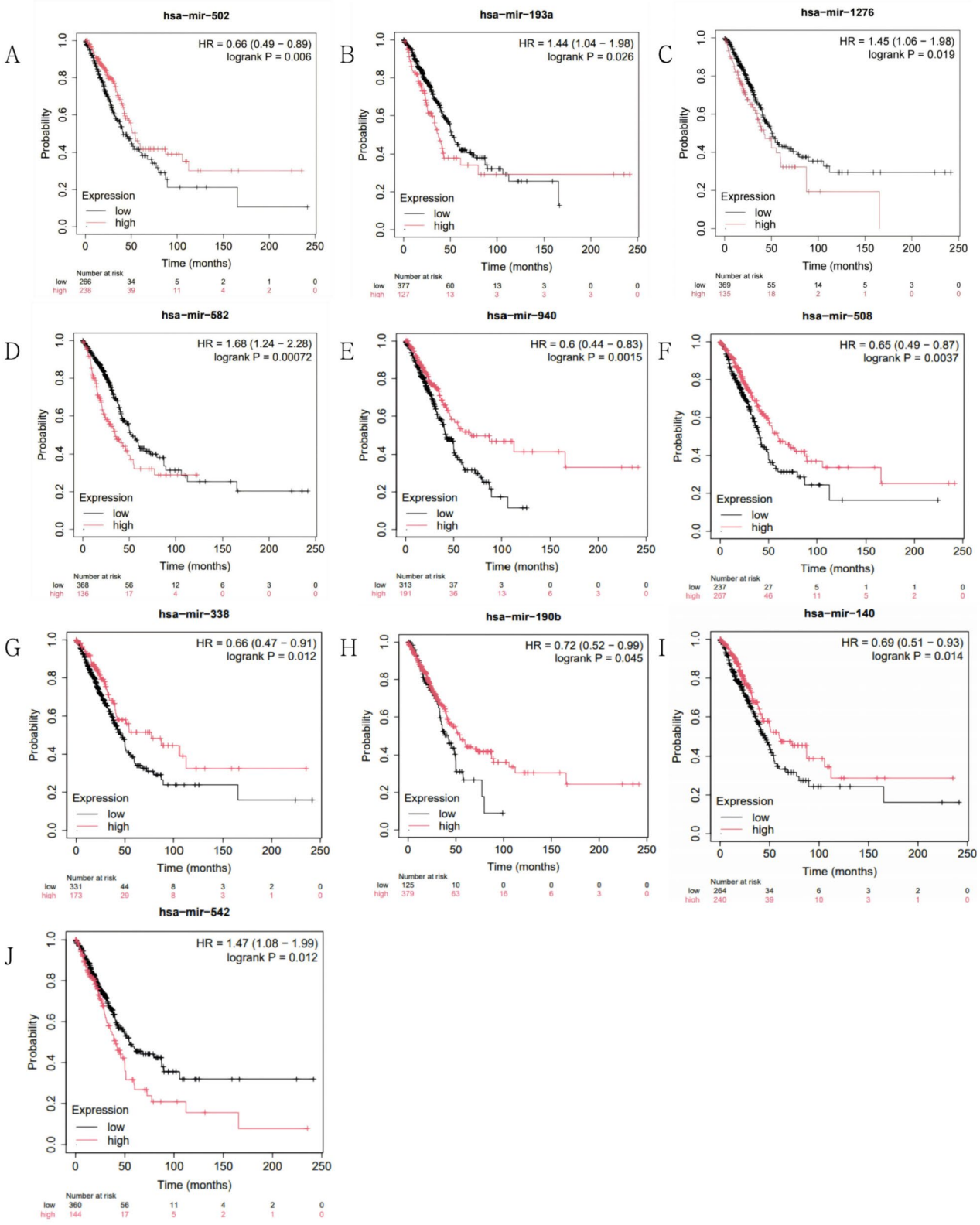

Fig. 2 **A-J** was used to predict the targeted miRNA of DEcircrna using CircBank database, intersected with DMmiRNA, and then used Kaplan-Meier survival analysis to obtain meaningful miRNA

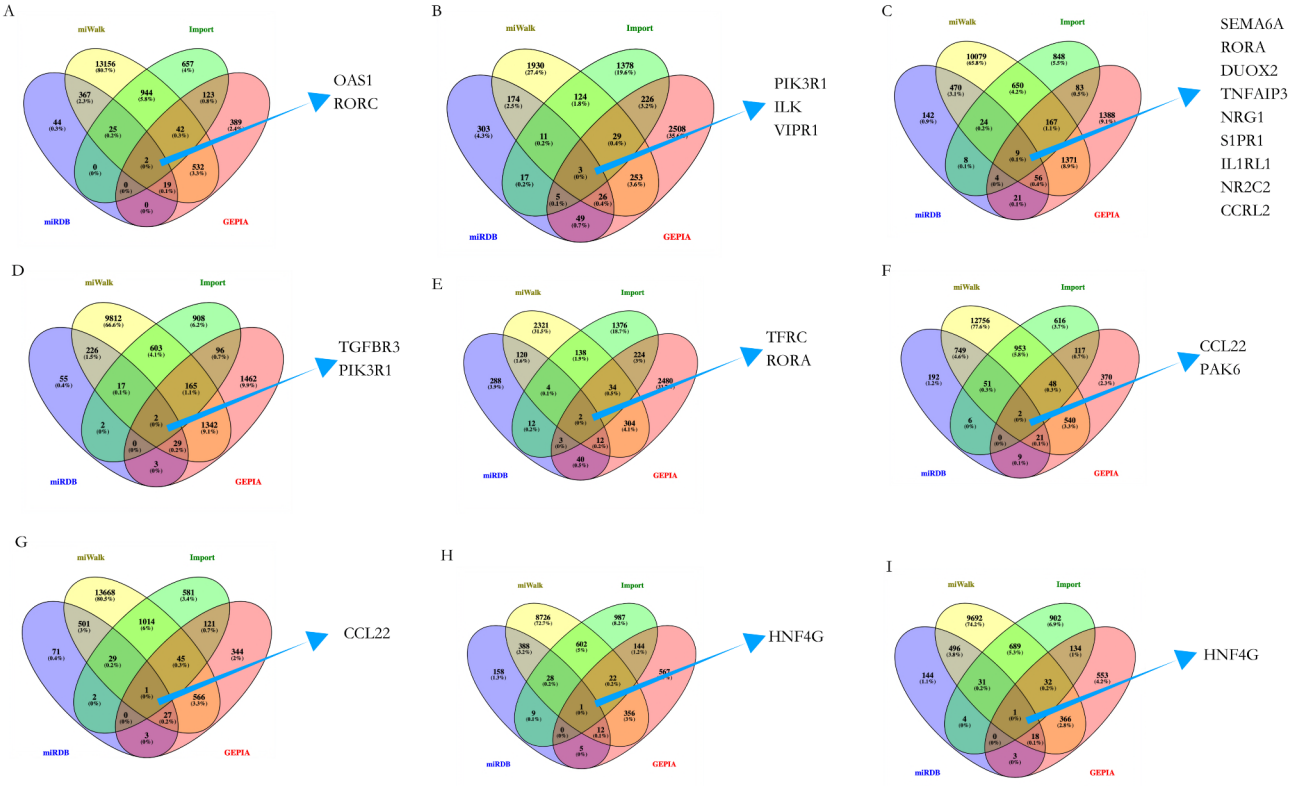

Fig. 3 **A-I** is the downstream mRNA prediction of meaningful miRNAs based on miWalk database and miRDB database and intersects with immune-related genes and DEmRNA from non-small cell lung cancer obtained from GEPIA online database

To investigate the impact of hsa_circ_0079557 on LUAD cells, we conducted experiments utilizing the A549 cell line. Initial validation of si-hsa_circ_0079557 knockdown efficiency is demonstrated in Fig. 8C. Subsequent colony formation assays revealed a significant reduction in proliferative capacity of hsa_circ_0079557-knockdown A549 cells compared to the negative control group (Fig. 8D). Consistent with this observation, CCK-8 assays confirmed that hsa_circ_0079557 knockdown markedly suppressed cellular proliferation (Fig. 8E). Furthermore, Transwell migration and invasion assays indicated diminished metastatic potential in hsa_circ_0079557-deficient A549 cells (Fig. 8F).

In summary, these experimental results fully illustrate that hsa_circ_0079557 plays a crucial role in the occurrence and development of LUAD.

Knockdown of Hsa_circ_0079557 Affects EMT Progression in LUAD Cells

Epithelial-mesenchymal transition (EMT) is a critical process by which epithelial cells acquire migratory and invasive capabilities. Therefore, we further investigated whether hsa_circ_0079557 affects the migratory ability of lung LUAD cells by regulating the expression of EMT-related proteins. Specifically, we examined the expression levels of three key EMT markers—E-cadherin, N-cadherin, and Vimentin—in LUAD cells with knockdown of hsa_circ_0079557. Western Blot experimental results showed that after knockdown of hsa_circ_0079557, the expression level of E-cadherin was significantly increased, while the expression levels of N-cadherin and Vimentin were decreased (Fig. 8G). This result strongly suggests that hsa_circ_0079557 plays a crucial role in enhancing the migratory and invasive abilities of LUAD cells by regulating the EMT process.

Discussion

Lung cancer is recognized as the most prevalent form of cancer globally. Due to the insidious nature of its clinical symptoms and the challenges associated with early detection, a significant number of patients are diagnosed at advanced stages of the disease [13]. The investigation into circRNA-mediated regulatory networks in LUAD remains insufficient, underscoring the critical need to explore the underlying molecular mechanisms of LUAD to improve diagnostic and therapeutic strategies. In this study, we analyzed LUAD expression data obtained from the GEO and TCGA databases to identify DEcircRNAs, DEmiRNAs, and DEmRNAs between LUAD tissues and adjacent normal tissues. By integrating the interactions between DEmiRNAs and either DEmRNAs or DEcircRNAs, we constructed a LUAD-specific regulatory

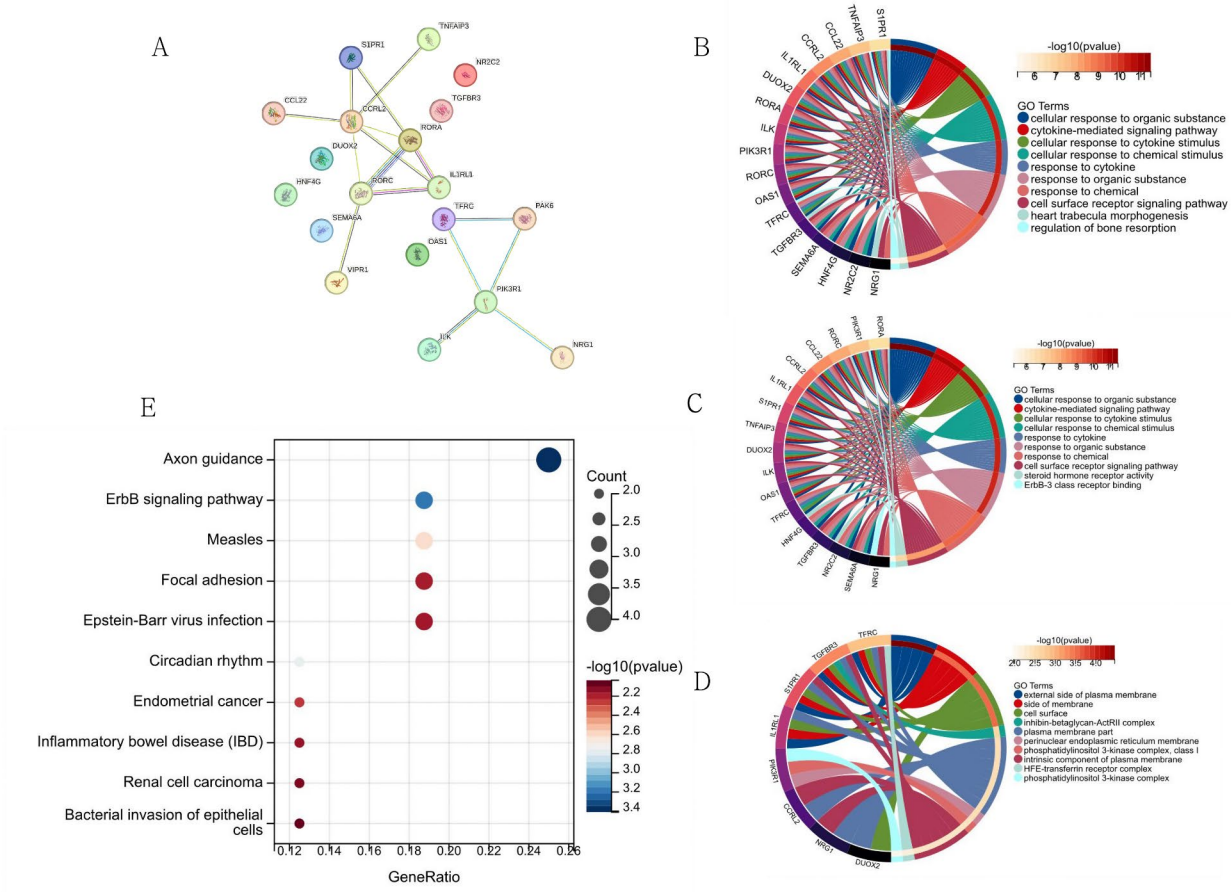

Fig. 4 Construction of PPI regulatory network and functional enrichment analysis. (**A**) PPI regulatory network of DEmRNAs. (**B-D**) The first 10 important GO enrichment annotations of genes, including BP, CC, MF. (**E**) Top 10 important KEGG pathways

network. GO and KEGG analyses were performed on the identified DEmRNAs, revealing that ceRNA-related RNAs predominantly engage in biological processes associated with hormone binding. KEGG enrichment analysis indicated significant involvement in the ErbB signaling pathway. We also conducted prognostic survival analyses on the identified DEmiRNAs and DEmRNAs, ultimately establishing a meaningful regulatory network.

Our findings indicate that Hsa_circ_0079557 is upregulated in colorectal cancer (CRC) tissues and cell lines, and its inhibition leads to a reduction in cell proliferation both in vitro and in vivo. Furthermore, Hsa_circ_0079557 functions as a "molecular sponge" for miR-502-5p, resulting in the upregulation of cyclin D1 (CCND1) expression [14]. However, there is a lack of reports concerning hsa_circ_0070100 in the context of lung cancer. This study proposes that hsa_circ_0079557 may influence the progression of lung adenocarcinoma through the hsa_circ_0079557-hsa-miR-502-5p-OAS1 axis. Additionally, hsa_circ_0020390 is found to be upregulated in bladder cancer (BC) tissues and cell lines, with its inhibition leading to decreased cell viability, suppressed proliferation, and reduced migratory potential of BC cells. Hsa_circ_0020390 exerts its effects by modulating the hsa_circ_0020390/hsa-miR-132-3p/Sox5 pathway in BC cells [15]. Research has shown that hsa_circ_0020390 promotes breast cancer progression by downregulating NEK2 through targeting miR-128-3p, suggesting that the hsa_circ_0020390/hsa-miR-128-3p/NEK2 axis may represent a novel therapeutic target for breast cancer treatment [16]. Furthermore, hsa_circ_0020390 has been implicated in the progression of osteosarcoma by regulating LEF1 as a competing endogenous RNA (ceRNA) for miR-936 [17]. Hsa_circ_0001666 has been identified as a tumor suppressor in esophageal squamous cell carcinoma via the miR-661/PPM1L axis and the PKR/p38 MAPK/EMT pathway [18]. Additionally, Hsa_circ_0001666 has been shown to inhibit colorectal cancer progression through the miR-576-5p/PCDH10 axis [19]. In lung cancer, circ0001666 is overexpressed in NSCLC cell lines and tissues, promoting cell migration and invasion both in vitro and in vivo [20]. Currently, there are no reports regarding hsa_circ_0023685, hsa_circ_0000370, and hsa_circ_0000369. This study is the first to suggest that these circRNAs may have potential regulatory roles in LUAD through ceRNA networks.

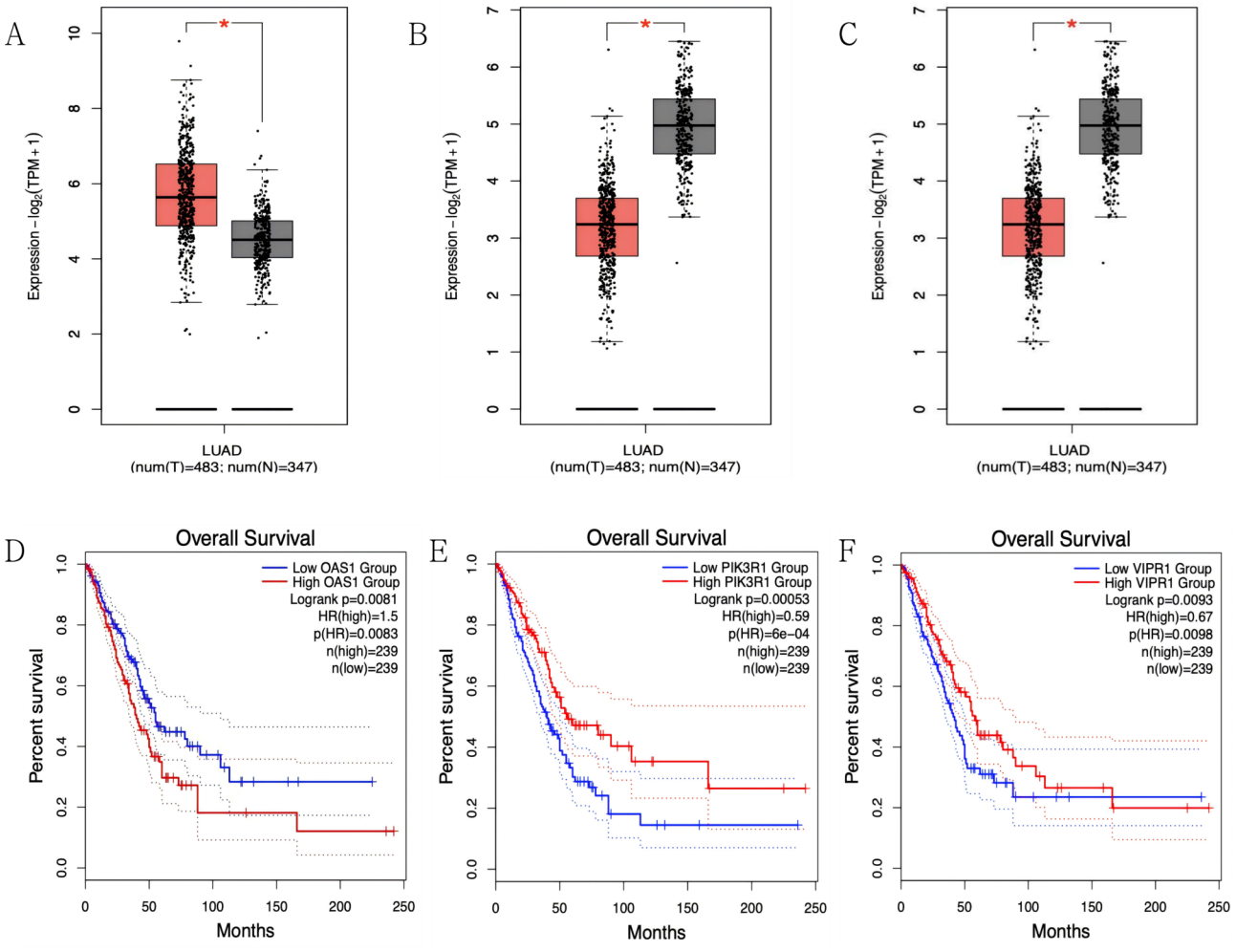

Fig. 5 The box plot shows the expression levels of 3 target genes between LUSC (TCGA database) and normal samples using GEPIA, as well as survival analyses. **A-C** is the expression level of OAS1, PIK3R1 and VIPR1 in TCGA database. **D-F** is survival analysis of OAS1, PIK3R1 and VIPR1 in TCGA database

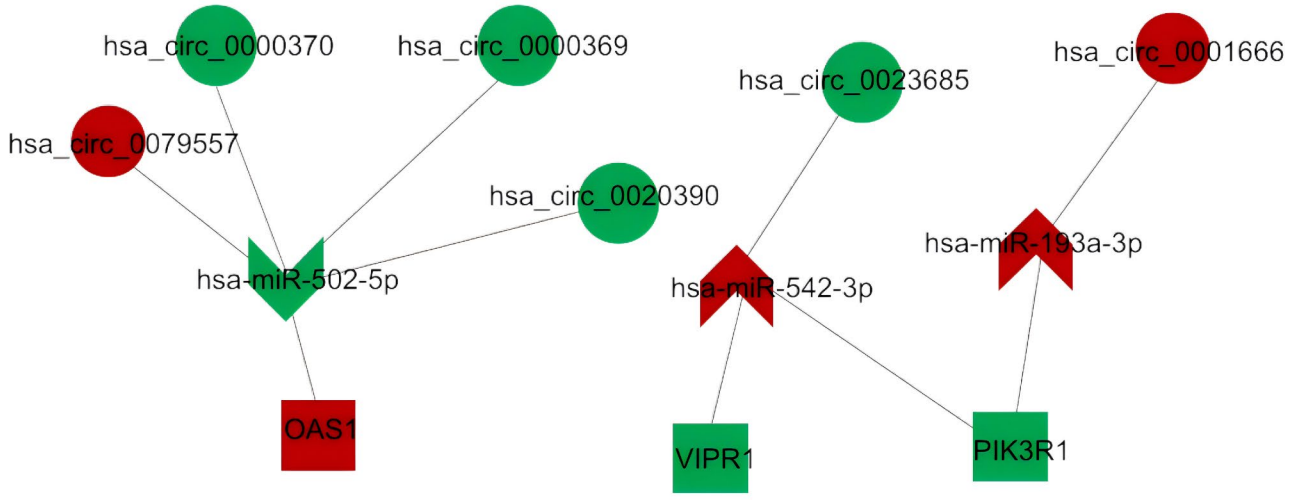

Fig. 6 circRNAs-miRNAs-mRNAs network. circRNA is represented as a circle, miRNA is represented as a hexagonal arrow, and mRNA is represented as a square blue. Green is down, red is up. The edges (lines) represent the relationship between circRNA, miRNA, and mRNA

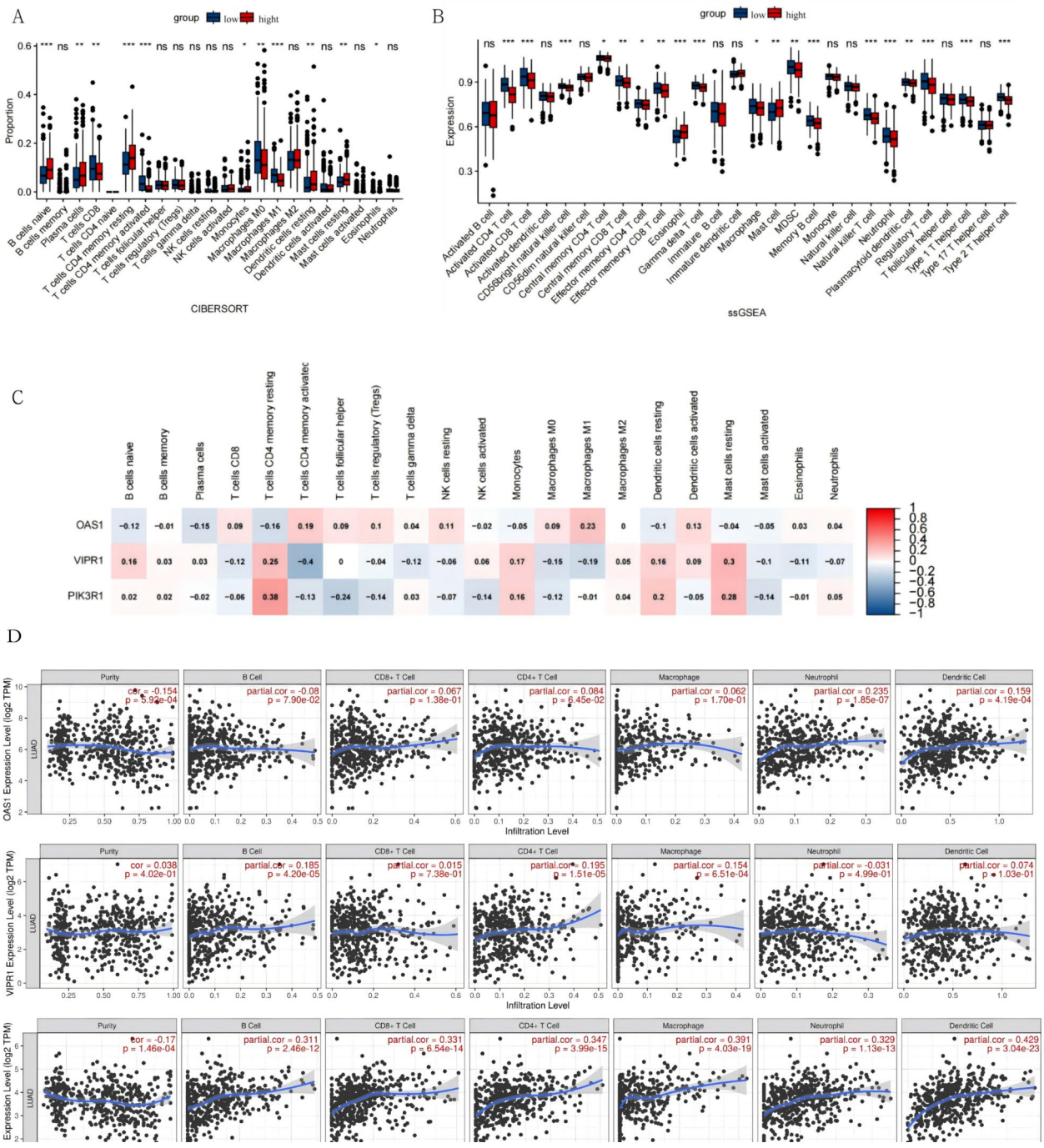

Fig. 7 Correlation between immune cell infiltration and hub immune-related DEmRNAs. (**A-B**) Distribution of immune cells in LUAD (red and green represent LUAD and control, respectively). (**C**) Pearson correlation between immune cell infiltration and hub immune-related DEmRNAs. * represent $P < 0.05$; ** represent $P < 0.01$; *** represent $P < 0.001$; **** represent $P < 0.0001$. (**D**) The correlation between the expression of "OAS1"、"PIK3R1" and "VIPR1" and tumor-infiltrating immune cells was analyzed

Research indicates that miR-502-5p functions as a tumor suppressor in gastric cancer (GC) [21], and the miR-502-5p/PD-L1 axis may represent a novel therapeutic target in GC treatment. MiR-502-5p has also been shown to inhibit ovarian cancer development by downregulating subunit 2 of the GINS complex [22]. Moreover, the downregulation of miR-502-5p significantly reverses the inhibitory effects of circNT5E silencing on the growth and migration of bladder cancer cells [23]. MiR-542-3p targets CDK14, inhibiting cell proliferation, invasiveness, and tumorigenesis in epithelial ovarian cancer [24]. Previous studies have suggested that serum levels

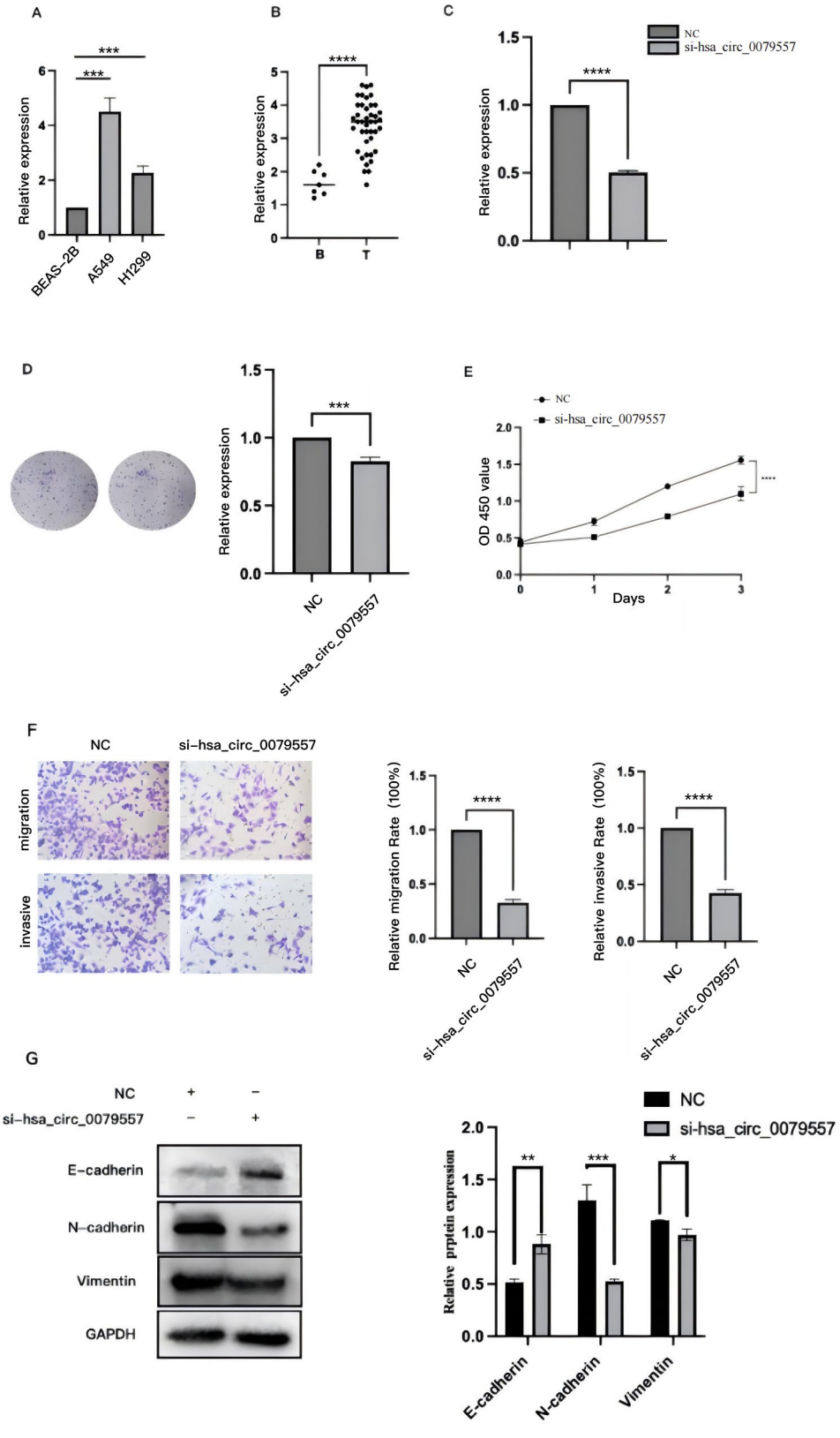

Fig. 8 (See legend on next page.)

(See figure on previous page.)

Fig. 8 The impact of knocking down hsa_circ_0079557 on the proliferation, invasion, migration, and epithelial-mesenchymal transition (EMT) of LUAD cells. (**A**) When compared to normal BEAS-2B cells, a notable discrepancy in the expression level of hsa_circ_0079557 is observed within LUAD cells. (**B**) Analysis of the expression levels of hsa_circ_0079557 in blood samples collected from patients, utilizing qPCR. (**C**) Validation of hsa_circ_0079557 knockdown efficiency by qPCR assay. (**D**) Assessment of hsa_circ_0079557 knockdown effects on cellular proliferative capacity using CCK-8 assay. (**E**) Experimental verification of hsa_circ_0079557's regulatory role in LUAD cells via plate colony formation assay. (**F**) Transwell migration assay demonstrating hsa_circ_0079557-mediated effects on LUAD cell motility. (**G**) Western blot analysis confirming hsa_circ_0079557's modulation of epithelial-mesenchymal transition (EMT) markers in LUAD cells

of miR-542-3p can serve as non-invasive blood biomarkers for tumor monitoring and prognosis prediction in osteosarcoma patients [25]. Additionally, miR-542-3p can inhibit cell proliferation and invasion by targeting KDM1A and ZNF346 in neuroblastoma, providing a theoretical foundation for neuroblastoma treatment [26]. Bin Liu et al. discovered that miR-542-3p acts as a suppressor gene by targeting and upregulating FTSJ2, thereby inhibiting the malignancy of NSCLC cells [27]. The tumor suppressor miR-193a-3p enhances the efficacy of BRAF/MEK inhibitors in BRAF-mutated colorectal carcinoma. The incorporation of miR-193a-3p with EGFR/BRAF/MEK inhibitors and/or modulation of proteins involved in miR-193a-3p-mediated pathways, such as Mcl1, may represent potential therapeutic strategies for BRAF-mutated CRC [28]. Furthermore, miR-193a-3p can inhibit the proliferation of pancreatic ductal adenocarcinoma cells by targeting CCND1 [29]. Investigators have found that the inhibition of ERBB4 by miR-193a-3p suppresses the proliferation and invasion of lung cancer cells while promoting apoptosis, with miR-193a-3p exerting an anti-tumor effect by negatively regulating ERBB4 in xenograft models [30]. Additionally, LncRNA-UCA1 has been shown to play an oncogenic role in NSCLC by targeting miR-193a-3p [31].

OAS1 (2′, 5′-oligoadenylate synthetase 1) is a key member of the OAS family and serves as a crucial antiviral enzyme induced by interferon [32, 33]. This gene family includes OAS1, OAS2, OAS3, and OASL. OAS1 is one of the most extensively studied members of the OAS family and plays a significant role in regulating immune responses [34, 35]. Research has indicated that OAS1 may serve as a molecular biomarker for the prognosis of various cancer types and could play a vital role in the tumor immune response [36]. Furthermore, a comprehensive single-cell analysis of LUAD has characterized tumor heterogeneity and the immune microenvironment, revealing that lung cancer patients with elevated OAS1 expression have a poor prognosis [37]. Vasoactive intestinal peptide (VIP), also known as PACAP, exerts its effects primarily through two receptor subtypes, VAPC1 (VIPR1) and VAPC2 [38]. Studies have suggested that reduced VIP levels may be associated with disease progression, and that VIP or VPAC1 receptor antagonists can enhance the efficacy of chemotherapy in eradicating breast cancer cells [39, 40]. In LUAD, low expression of VIPR1 correlates with poor prognosis, and it has been reported that VIPR1 may function as a tumor suppressor gene in the pathogenesis of human LUAD [41]. Phosphatidylinositol 3-kinase (PI3K) activity is stimulated by various oncogenes and growth factor receptors, with aberrations in PI3K signaling considered a hallmark of cancer [42]. PIK3R1 (phosphoinositide-3-kinase regulatory subunit 1), which encodes P85α, the principal regulatory subunit of class I PI3K, inhibits the catalytic activity of P110α kinase, binds directly to PTEN, and enhances lipid phosphatase activity [43]. Studies have demonstrated that low PIK3R1 expression is associated with poor prognosis across multiple cancer types [44]. It has been revealed that PIK3R1 expression is significantly diminished in lung cancer datasets, with low expression correlating with tumor grade, family history of cancer, the presence of multiple tumors, and prior lung cancer treatment [45]. Additionally, it has been discovered that the downregulation of miR-486-5p is negatively correlated with the upregulation of its direct target gene PIK3R1, and the overexpression of miR-486-5p inhibits NSCLC cell proliferation and invasion [46].

Despite the establishment of a LUAD-specific regulatory network and the identification of potential prognostic biomarkers, certain limitations remain. Firstly, this study relies exclusively on gene expression data sourced from databases. Future prospective studies involving diverse populations and larger patient cohorts are necessary to validate our findings. Secondly, our study does not incorporate clinical characteristics of LUAD patients, such as TNM staging and gene mutations. Lastly, additional experimental investigations will be required to elucidate the potential biological mechanisms underlying these regulatory networks in LUAD.

In conclusion, in this study, we have identified several circRNA-miRNA-immune-related mRNA axes that potentially play pivotal regulatory roles in lung adenocarcinoma (LUAD). Specifically, hsa_circ_0079557, hsa_circ_0000370, hsa_circ_0000369, hsa_circ_0020390, hsa_circ_0023685, hsa_circ_0001666, along with miRNAs such as hsa-miR-502-5p, hsa-miR-193a, and hsa-miR-542-3p, and mRNAs including OAS1, VIPR1, and PIK3R1, exhibit potential clinical utility as prognostic indicators or novel biomarkers in LUAD. Among these, we have selected hsa_circ_0079557, a circRNA, for further validation. However, it is noteworthy that despite the biological significance demonstrated by these circRNAs, miRNAs, and mRNAs in LUAD, their specific functions

and underlying mechanisms still require in-depth investigation and validation. A comprehensive understanding of the biological characteristics of these molecules and their specific roles in the initiation and progression of LUAD is essential for accurately assessing their potential as novel biomarkers or therapeutic targets for LUAD patients, thereby providing novel insights and methodologies for improving the diagnosis and treatment of LUAD.

Supplementary Information

The online version contains supplementary material available at https://doi.org/10.1186/s12575-025-00275-4.

Supplementary Material 1

Supplementary Material 2

Acknowledgements
Not applicable.

Author Contributions
H.Y. Li, responsible for data analysis, manuscript writing, and experimental conduct; X. Jin, responsible for data analysis and sorting, and article writing; W. Li, responsible for writing the article and data collation; F. Ren, T. Li, X.G. Li, and H.C. Yu were responsible for data collation and collection. D.X. Fu, responsible for data collection and sorting; S. XU, and Z.Q. Song provided funding as corresponding authors.

Funding
This study was funded by National Natural Science Foundation of China (82172776), Tianjin Health Research Project (TJWJ2023XK005), Tianjin Science and Technology Plan Project (24ZXGZSY00010, 24JCZDJC01030).

Data Availability
No datasets were generated or analysed during the current study.

Declarations

Ethics Approval and Consent for Publication
All experimental protocols were approved by the Ethics Committee of Tianjin Medical University General Hospital (IRB2024-YX-045-01) and were performed in accordance with relevant guidelines and regulations. All patients had been informed and signed informed consent prior to the experiment.

Competing Interests
The authors declare no competing interests.

Author details
[1]Department of Lung Cancer Surgery, Tianjin Medical University General Hospital, Tianjin, China
[2]Tianjin Key Laboratory of Lung Cancer Metastasis and Tumor Microenvironment, Lung Cancer Institute, Tianjin Medical University General Hospital, Tianjin, China
[3]Department of Radiology, Tianjin Key Laboratory of Functional Imaging, Tianjin Medical University General Hospital, Tianjin 300052, China

Received: 8 February 2025 / Accepted: 24 March 2025
Published online: 10 April 2025

References

1. Kerdidani D, et al. Wnt1 silences chemokine genes in dendritic cells and induces adaptive immune resistance in lung adenocarcinoma. Nat Commun. 2019;10(1):1405.
2. Qin H, et al. New advances in immunotherapy for non-small cell lung cancer. Am J Transl Res. 2018;10(8):2234–45.
3. Sanger HL, et al. Viroids are single-stranded covalently closed circular RNA molecules existing as highly base-paired rod-like structures. Proc Natl Acad Sci U S A. 1976;73(11):3852–6.
4. Jeck WR, Sharpless NE. Detecting and characterizing circular RNAs. Nat Biotechnol. 2014;32(5):453–61.
5. Hong W, et al. Circular RNA circ-CPA4/ let-7 miRNA/PD-L1 axis regulates cell growth, stemness, drug resistance and immune evasion in non-small cell lung cancer (NSCLC). J Exp Clin Cancer Res. 2020;39(1):149.
6. Fan Z, et al. CircRNA circ_POLA2 promotes lung cancer cell stemness via regulating the miR-326/GNB1 axis. Environ Toxicol. 2020;35(10):1146–56.
7. Liu Z, et al. N(6)-methyladenosine-modified circIGF2BP3 inhibits CD8(+) T-cell responses to facilitate tumor immune evasion by promoting the deubiquitination of PD-L1 in non-small cell lung cancer. Mol Cancer. 2021;20(1):105.
8. Remark R, et al. The non-small cell lung cancer immune contexture. A major determinant of tumor characteristics and patient outcome. Am J Respir Crit Care Med. 2015;191(4):377–90.
9. Li Y, et al. UPP1 promotes lung adenocarcinoma progression through the induction of an immunosuppressive microenvironment. Nat Commun. 2024;15(1):1200.
10. Exposito F, et al. PTEN loss confers resistance to Anti-PD-1 therapy in Non-Small cell lung cancer by increasing tumor infiltration of regulatory T cells. Cancer Res. 2023;83(15):2513–26.
11. Panda AC. Circular RNAs act as MiRNA sponges. Adv Exp Med Biol. 2018;1087:67–79.
12. Thomson DW, Dinger ME. Endogenous MicroRNA sponges: evidence and controversy. Nat Rev Genet. 2016;17(5):272–83.
13. Gridelli C, et al. Non-small-cell lung cancer. Nat Rev Dis Primers. 2015;1:15009.
14. Yu C, et al. Hsa_circ_0079557 promotes the proliferation of colorectal cancer cells through the hsa_circ_0079557/miR-502-5p/CCND1 axis. Cancer Genomics Proteom. 2023;20(6):567–81.
15. Liu P et al. Circular RNA DOCK1 promotes bladder carcinoma progression via modulating circDOCK1/hsa-miR-132-3p/Sox5 signalling pathway. Cell Prolif, 2019. 52(4): p. e12614.
16. Ni Z, et al. Circular forms of dedicator of cytokinesis 1 promotes breast cancer progression by derepressing never in mitosis related kinase 2 via sponging miR-128-3p. Environ Toxicol. 2023;38(7):1712–22.
17. Xu G, et al. Circular RNA circDOCK1 contributes to osteosarcoma progression by acting as a CeRNA for miR-936 to regulate LEF1. J Bone Oncol. 2022;36:100453.
18. Song H, et al. circFAM120B functions as a tumor suppressor in esophageal squamous cell carcinoma via the miR-661/PPM1L axis and the PKR/p38 MAPK/EMT pathway. Cell Death Dis. 2022;13(4):361.
19. Zhou J, et al. Hsa_circ_0001666 suppresses the progression of colorectal cancer through the miR-576-5p/PCDH10 axis. Clin Transl Med. 2021;11(11):e565.
20. Wang X, et al. Hsa_circ_0001666 promotes non-small cell lung cancer migration and invasion through miR-1184/miR-548l/AGO1 axis. Mol Ther Oncolytics. 2022;24:597–611.
21. You W, et al. miR-502-5p affects gastric cancer progression by targeting PD-L1. Cancer Cell Int. 2020;20:395.
22. Zhan L, et al. MicroRNA miR-502-5p inhibits ovarian cancer genesis by downregulation of GINS complex subunit 2. Bioengineered. 2021;12(1):3336–47.
23. Yang J, et al. CircNT5E promotes the proliferation and migration of bladder cancer via sponging miR-502-5. J Cancer. 2021;12(8):2430–9.
24. Li J, Shao W, Feng H. MiR-542-3p, a MicroRNA targeting CDK14, suppresses cell proliferation, invasiveness, and tumorigenesis of epithelial ovarian cancer. Biomed Pharmacother. 2019;110:850–6.
25. Li Q, et al. Serum miR-542-3p as a prognostic biomarker in osteosarcoma. Cancer Biomark. 2018;21(3):521–6.
26. Wei Q, et al. MiR-542-3p suppresses neuroblastoma cell proliferation and invasion by downregulation of KDM1A and ZNF346. Open Life Sci. 2020;15:173–84.
27. Liu B, et al. MiR-542-3p exerts tumor suppressive functions in non-small cell lung cancer cells by upregulating FTSJ2. Life Sci. 2017;188:87–95.
28. Hiraide S, et al. Tumor suppressor miR-193a-3p enhances efficacy of BRAF/MEK inhibitors in BRAF-mutated colorectal cancer. Cancer Sci. 2021;112(9):3856–70.
29. Chen ZM, et al. MiR-193a-3p inhibits pancreatic ductal adenocarcinoma cell proliferation by targeting CCND1. Cancer Manag Res. 2019;11:4825–37.
30. Liang H, et al. miR-193a-3p functions as a tumor suppressor in lung cancer by down-regulating ERBB4. J Biol Chem. 2015;290(2):926–40.

31. Nie W, et al. LncRNA-UCA1 exerts oncogenic functions in non-small cell lung cancer by targeting miR-193a-3p. Cancer Lett. 2016;371(1):99–106.
32. Hovanessian AG, Justesen J. The human 2′-5′oligoadenylate synthetase family: unique interferon-inducible enzymes catalyzing 2′-5′ instead of 3′-5′ phosphodiester bond formation. Biochimie. 2007;89(6–7):779–88.
33. Rebouillat D, Hovanessian AG. The human 2′,5′-oligoadenylate synthetase family: interferon-induced proteins with unique enzymatic properties. J Interferon Cytokine Res. 1999;19(4):295–308.
34. Junghare V, et al. In Silico modeling revealed new insights into the mechanism of action of enzyme 2′-5′-oligoadenylate synthetase in cattle. J Biomol Struct Dyn. 2022;40(24):14013–26.
35. Fish I, Boissinot S. Functional evolution of the OAS1 viral sensor: insights from old world primates. Infect Genet Evol. 2016;44:341–50.
36. Jiang S, et al. Pan-cancer analysis identified OAS1 as a potential prognostic biomarker for multiple tumor types. Front Oncol. 2023;13:1207081.
37. Xu J, et al. A single-cell characterised signature integrating heterogeneity and microenvironment of lung adenocarcinoma for prognostic stratification. EBioMedicine. 2024;102:105092.
38. Szilasi M, et al. Gene expression of vasoactive intestinal peptide receptors in human lung cancer. Int J Oncol. 2011;39(4):1019–24.
39. Moody TW, et al. VIP receptor antagonists inhibit mammary carcinogenesis in C3(1)SV40T antigen mice. Life Sci. 2004;74(11):1345–57.
40. Moody TW, et al. VIP receptor antagonists and chemotherapeutic drugs inhibit the growth of breast cancer cells. Breast Cancer Res Treat. 2001;68(1):55–64.
41. Zhao L, Yu Z, Zhao B. Mechanism of VIPR1 gene regulating human lung adenocarcinoma H1299 cells. Med Oncol. 2019;36(11):91.
42. Fruman DA, et al. The PI3K pathway in human disease. Cell. 2017;170(4):605–35.
43. Urick ME, et al. PIK3R1 (p85alpha) is somatically mutated at high frequency in primary endometrial cancer. Cancer Res. 2011;71(12):4061–7.
44. Liu Y, et al. Pan-cancer analysis on the role of PIK3R1 and PIK3R2 in human tumors. Sci Rep. 2022;12(1):5924.
45. Chen Y, et al. Bioinformatics analysis screened and identified key genes as potential biomarkers for progression of lung cancer. J Coll Physicians Surg Pak. 2022;32(6):712–21.
46. Tian F, et al. MiR-486-5p serves as a good biomarker in nonsmall cell lung cancer and suppresses cell growth with the involvement of a target PIK3R1. Front Genet. 2019;10:688.

Publisher's Note